buildings

MDPI

Article

Weathering Mechanisms of Porous Marl Stones in Coastal Environments and Evaluation of Conservation Treatments as Potential Adaptation Action for Facing Climate Change Impact

Anastasia Michalopoulou [1,*], Iason Markantonis [2], Diamando Vlachogiannis [2], Athanasios Sfetsos [2], Vassilis Kilikoglou [1] and Ioannis Karatasios [1]

[1] Institute of Nanoscience and Nanotechnology, National Centre for Scientific Research "Demokritos", 15310 Athens, Greece
[2] Institute of Nuclear & Radiological Sciences & Technology, Energy & Safety, National Centre for Scientific Research "Demokritos", 15310 Athens, Greece
* Correspondence: a.michalopoulou@inn.demokritos.gr

Abstract: This work presents the methodological approach followed for the study of the interaction of natural stone monuments with the local microclimate (exposure to RH, temperature alterations, wind, marine aerosol). This was implemented with the documentation of the associated weathering phenomena and the study of historic climate data of the area. The paper is focused on the main weathering mechanisms of the marly limestone at the Hellenistic theater of Zea in Piraeus, Greece. Based on the weathering phenomena identified, the development of the appropriate mitigation strategy was based on the physical, chemical and mechanical characterization of the natural stones, along with the evaluation of different conservation treatments, considering the characteristics of the coastal environment. Considering the mineralogy of marly limestones, silane-based materials were selected for providing both consolidation and water repellency effects. The evaluation of the conservation treatments was based on the modification of microstructural and water-related properties of natural stone samples, along with their consequent effect on their durability against accelerated aging tests. The results indicated that the design of migration actions proved to be multivariable parameter, depending on the intrinsic stone properties, the environmental parameters and the conservation efficacy of the treatments.

Keywords: climate change; archaeological sites; stone monuments; historic climate data; mitigation; stone conservation; weathering phenomena; mineralogy; marly limestones

check for updates

Citation: Michalopoulou, A.; Markantonis, I.; Vlachogiannis, D.; Sfetsos, A.; Kilikoglou, V.; Karatasios, I. Weathering Mechanisms of Porous Marl Stones in Coastal Environments and Evaluation of Conservation Treatments as Potential Adaptation Action for Facing Climate Change Impact. *Buildings* **2023**, *13*, 198. https://doi.org/10.3390/buildings13010198

Academic Editor: Bruno Sena da Fonseca

Received: 12 December 2022
Revised: 31 December 2022
Accepted: 4 January 2023
Published: 11 January 2023

Copyright: © 2023 by the authors. Licensee MDPI, Basel, Switzerland. This article is an open access article distributed under the terms and conditions of the Creative Commons Attribution (CC BY) license (https://creativecommons.org/licenses/by/4.0/).

1. Introduction

The conservation planning and interventions of architectural and archaeological heritage are multilevel processes because they involve the study of the intrinsic characteristics of porous building materials; the structural analysis of the assets, including safety aspects; the interaction of materials with the surrounding environment; the identification of the main weathering mechanisms; and the preservation of structures with historical and cultural significance [1–7].

Natural stones have been widely used as building material for the construction of monuments, roof or paving and ornaments and sculptures [8–10]. According to the relevant literature [8,9,11], some of the most widely used natural stones are limestone, sandstone, marble, basalt, granite, slatestone, tuff, flint/cherts and obsidian.

The primary degradation mechanism detected in porous building materials are chemical dissolution and salt crystallization [12–14]. This is attributed to the initiation of chemical processes (controlled by active reactions) and the presence of water, resulting in modifications of both the surface characteristics and the internal cohesion of the natural stone [1,15].

The main factors that affect the weathering mechanisms are: the intrinsic properties and conservation state of the building material, climate change [16–18], the environmental parameters of the outdoor environment [19], the presence of unusual environmental episodes or natural disasters [20], the presence of anthropogenic pollutants [21] and human actions [22]. Furthermore, the hindrance of the weathering processes highly depends on the geographical and topographical traits of the archaeological contexts and the architectural characteristics of the stone monuments. Thus, the promotion of the sustainability of a stone monument depends on both the conservation state and the response of the historical structure as a whole [6,23,24]. In coastal archaeological sites, the main weathering mechanisms are initiated by the deposition and crystallization of soluble salts [25–27], caused by the transportation of marine aerosols [4,28–30]. The deposition and crystallization of various salts due to marine spray erosion and wind action lead to the activation of superficial decay phenomena, such as alveolization and development of crusts and efflorescence [25], or to the capillary rise of salt-enriched water, initiating the presence of internal mechanical stresses inside the porous substrate [27,31–36]. The crystallization pressure of the newly formed crystals disorders the microstructure of porous building materials, creates several micro-cracks and surface exfoliation. The crystallization pressure, and thus the damage associated, depends on (a) the porous network of the stone and (b) the degree of supersaturation of the solution, as well as (c) the salts volume upon crystallization [26,37–39]. The latter is strongly related to the environmental conditions (RH%, T °C) [40] and indicates the significant role of micro-climate on the evolution and aggressiveness of the weathering process.

In the above context, this work quantifies the occurrence of past salt crystallization events, based on historic data retrieved from local weather stations, in order to quantify soluble salts risks and understand the importance of this factor on the weathering phenomena that occurred at the stone material of the Hellenistic theater of Zea (200 B.C.). The archaeological site is located about 600 m north at Piraeus peninsula, about 500m east of Piraeus harbor and 100 m west of Zea harbor (Figure 1). The environment can be characterized as Csb (Köppen–Geiger climate classification) Mediterranean climate. The geological profile of the Piraeus peninsula includes formations from the Cenozonic era, such as deposits from the epochs of Pliocene, Pleistocene and Holocene river [41,42]. The three main lithic classes present include: (a) the Marls of Piraeus, including marly sandstones and limestones, conglomerates and marls with distinct inner layers of silicatic formations (clays, sands and siltstones), (b) the Cretaceous limestones and (c) the Holocene deposits (Figure 1).



Figure 1. Location and geological map of Piraeus. The red area consists of formations attributed to the Neogene Period (Pliocene and Pleistocene epochs) of the Cenozonic era [41].

Considering the elevated occurrence of seasonal salt crystallization events that follow the same trend historically, a further aim of this work is to evaluate the effectiveness of different conservation treatments as a potential adaptation measure for minimizing the aggressiveness of weathering mechanisms in the next years. Four different types of silane-based materials were studied for this purpose, aiming to examine both their consolidation and water repellency effects. The evaluation of the conservation treatments was based on

the modification of microstructural and water-related properties of natural stone samples, along with their consequent effect on their durability against accelerated aging tests.

The main aim is to contribute towards the determination of the parameters directly affecting the development of a mitigation strategy against the weathering phenomena and the design of a restoration plan of action regarding architectural lithic monuments of coastal archaeological contexts. The present study aspires to determine, monitor and predict the durability of Marl of Piraeus in relation with their physicochemical, petrological and micro-structural properties and the characteristics of the local microclimate. It is anticipated that the interpretation of the results could lead to the future design of an appropriate conservation plan of the stone material and mitigation action towards the weathering phenomena.

2. Materials and Methods

2.1. Seasonal Quantification of Salt Transition Events

In order to study the impact of weather conditions on the monument, we have calculated the number of events that favor the crystallization of salts. Consequently, validated data on a daily basis were derived from the meteorological station operated by the Hellenic National Meteorological Service (HNMS), named "Athens-Hellinikon" for the period 1980–2004. The meteorological station is located close to the coast of Saronikos Gulf, which is nearest to the point of interest. The variables extracted are the minimum and maximum values of daily relative humidity (minRH, maxRH), and they were used for the calculation of the number of salt transition events. The minimum and maximum values of daily relative humidity (minRH, maxRH) directly affect the crystallization of halite, which is the focal point of this study. An event of crystallization of halite occurs when min. RH (%) is lower than 75.3% and maxRH higher than 75.3% [2]. Accordingly, we have obtained the number of salt transition events on a seasonal basis. In this manner, the season that yields a higher risk for the surface of monuments can be revealed.

2.2. Stone Samples and Conservation Materials

Seven types of marly limestone stone samples were selected and collected from the different architectural parts of the theater for the implementation of laboratory-scale experiments representative of the geological surface formations of the natural stones used in the Hellenistic theater of Zea, according to historical evidence [25]. The selection of the natural stone samples was based on the appearance of similar weathering profiles, followed by petrographic examination, mineralogical analysis and mechanical properties. Cubic (40 × 40 × 40 mm) and prismatic (40 × 40 × 160 mm) specimens were prepared from larger natural stone fragments.

2.3. Conservation Products-Application Procedure

Four different types of silane-based materials were selected, divided into: (a) ethyl-silicate-based consolidants (Wacker BS OH-100, a tetraethyl-orthosilicate (TEOS) consolidant with an active content ~100 % (BS OH-100) and Remmers KS 300HV, a tetra-ethyl silicate (TEOS) with active content ~95 % (KS 300HV)) and (b) water repellents (Remmers Funcosil SL, an alkyl-alkoxy silane solution of active content ~7 % (Funcosil SL) and Wacker SILRES BS 1001, a silane-siloxane mixture of a solventless emulsion, with active content ~10 %, diluted to 1:4 in de-ionized water (BS 1001). The action of the silane-based materials is based on the formation and deposition of the amorphous silica gel, through the hydrolysis of silanes by water (for the formation of the intermediate chemical compound, silanols (–Si–OH)) and their condensation, resulting in the formation of silica gel, which attributes the required strength to the stone [43–47].

All treatments were carried out by capillary absorption, as a time-controlled [48] and easily reproducible laboratory-scale procedure [49] (Figure 2). All stone specimens were previously washed with deionized water, left to dry until constant weight at 40 ± 5 °C, and then kept under laboratory conditions for 2 h. Each side of the cubic stone specimens

was placed in direct contact with the material for 30 min, in order to ensure penetration by capillary forces [48]. Upon completion of the above procedure, all specimens were stored in a ventilated box under controlled laboratory conditions (T = 22 °C ± 2 °C, RH = 65–70%). The curation time was estimated at 8 weeks, according to previous studies concerning the completion of the polymerization reaction [50].



Figure 2. Representative stone specimens used in this work indicating the treatment of stone specimens via capillary absorption.

2.4. Physicochemical Characterization

The microstructural characterization of all natural stone specimens was carried out through petrographic examination and surface morphology. The petrographic examination was implemented under the petrographic microscope with corresponding thin sections in crossed Nichols, for the determination of fabric and microstructure and microstructural/morphological. The freshly fractured surfaces were examined with the use of a Scanning Electron Microscope coupled with an Energy Dispersive X-ray analyzer (SEM/EDX) (Fei, Eindhoven, Netherlands). The fractured stone samples were deposited on SEM-holders and were carbon-coated prior to the examination. SEM images were collected in a FEI Quanta Inspect instrument operated at 25 kV.

The mineralogical characterization of the stone samples was implemented by y X-ray powder diffraction (XRD), in a Siemens D-500 diffractometer, using Cu-Kα radiation (λ = 1.5406 Å) (Siemens, Zug, Switzerland)). The diffractograms were collected in the range of 5–55° 2θ scale, with a step of 0.03°/3 s. Moreover, the water-transport-related properties of water absorption and the capillary absorption coefficient of cubic stone samples (40 × 40 × 40 mm) were calculated according to EN 1925:1999.

The conductivity measurements were implemented with the use of an electrical conductivity meter. Two grams of the specimens were grounded and dissolved in 100 mL of de-ionized water. After the stirring of the solution for 10 min and the precipitation of the solid material, the conductivity of the aqueous solution was estimated.

2.5. Accelerating Aging Test

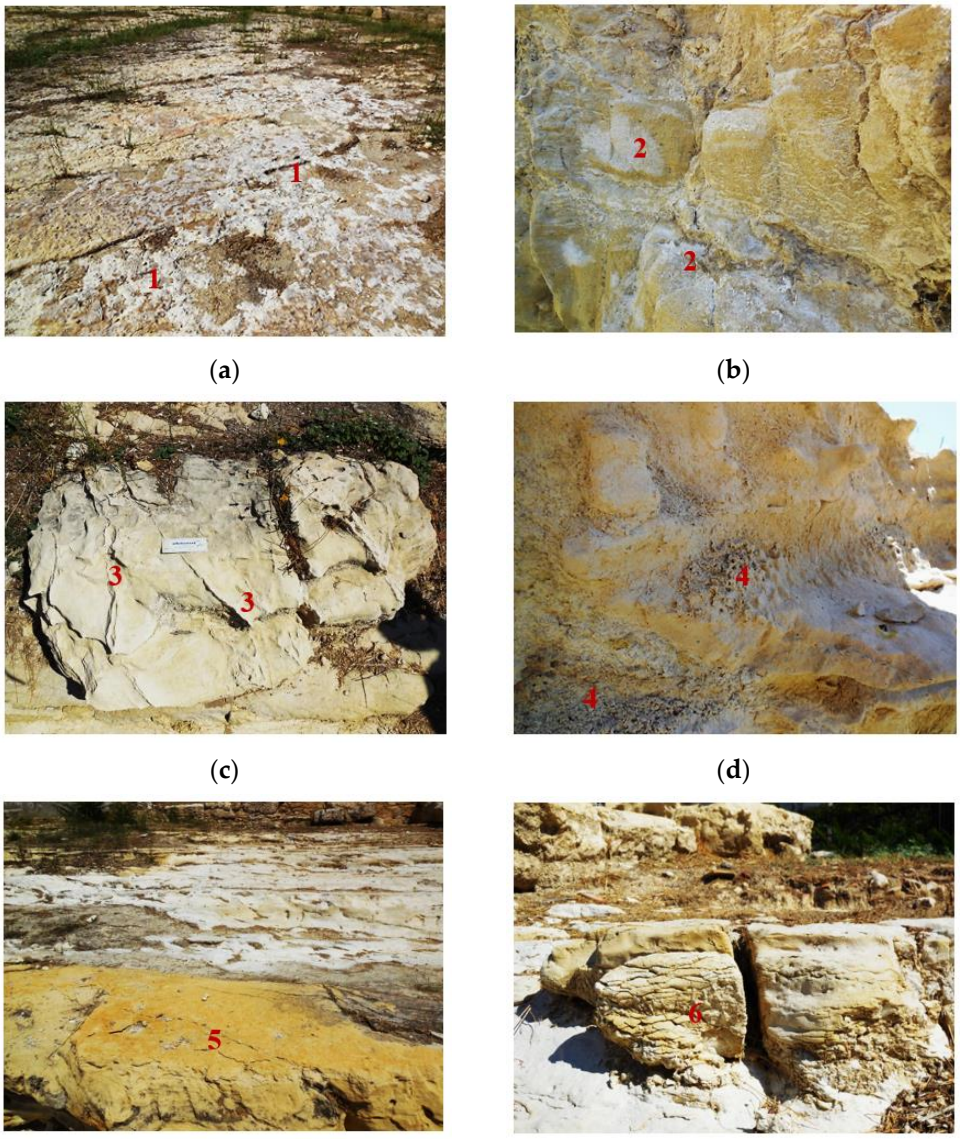
Aiming to determine the durability of different stone samples against salt crystallization, both reference and treated stone specimens from each category were subjected to continuous crystallization cycles with sodium chloride (NaCl). The specimens were dried at 55 ± 5 °C until constant mass and then immersed in an aqueous solution of NaCl (14% w/v) for 2 h. The selection of the single salt NaCl was based on the identification of NaCl as the primary degradation agent at the archaeological site. Both treated and reference stone specimens were removed from the salts solution and left to dry at 60 ± 5 °C for 22 h [51]. Each of the stone specimens were weighed before each of the 31 soaking cycles in the fresh sodium chlorite solution, for the estimation of their weight difference (ΔW%).

3. Results

3.1. Identification of Weathering Phenomena

The in situ survey of the site underlined the severe effects of soluble salts on the weathering processes of marly limestone. The main deterioration patterns identified were

divided into four categories [1,52]: (i) sea salt deposits and crusts (n.1 in Figure 3a), efflorescence and sub-fluorescence (n.2 in Figure 3b); (ii) differential erosion (n.3 in Figure 3c) and alveolization (honeycombs) (n.4 in Figure 3d); (iii) exfoliations (n.5 in Figure 3e), cracks induced from clay swelling (n.6 in Figure 3f), spalling and splitting (n.7 in Figure 3g); and (iv) biological and colonization (n.8 in Figure 3h). The seven stone samples presented variable cohesion per layer, an intense network of visible and invisible cracks, and an increased amount of soluble salts (NaCl) in the layers close to the surface (1–2 cm).



(**a**) (**b**)

(**c**) (**d**)

(**e**) (**f**)

Figure 3. *Cont.*



(**g**) (**h**)

Figure 3. In situ identification of weathering phenomena: (i) sea-salt deposits and crusts (**a**), efflorescence and sub-fluorescence (**b**); (ii) differential erosion (**c**) and alveolization (honeycombs) (**d**); (iii) exfoliations (**e**), cracks induced from clay swelling (**f**), spalling and splitting (**g**); and (iv) biological and colonization (**h**).

3.2. Seasonal Quantification of Salt Transition Events

Figure 4 indicated a sinusoidal variation of the total number of annual crystallization events that maintains a very high risk. The higher risk of the occurrence of crystallization events was attributed to the characteristics of the microclimate, specifically the variations of RH and temperature with a constant and repeatable rate. Specifically, according to Figure 4, the number of crystallizations of halite events per season was lower during summer in the area, compared to the higher values detected during spring and winter. The low values of halite crystallization events during the summer period were attributed to the higher values of temperature and relatively low values of RH. On the contrary, the increased values of events during spring were attributed to the increase in the temperature and the variations of RH values. Likewise, the increased values during the winter season were attributed to the higher levels of RH in the area of interest. An inter-annual variation due to climate variability could also be concluded, with some years presenting a higher number of events causing the crystallization of halite.

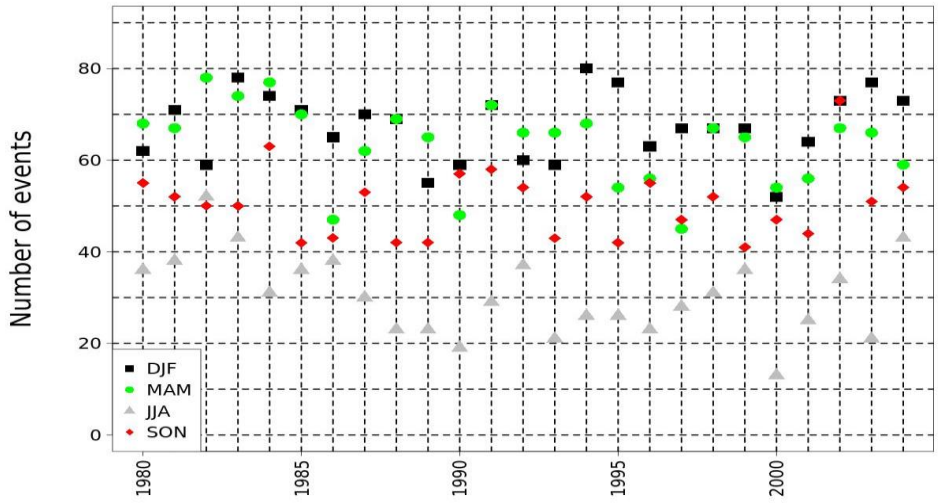


Figure 4. Quantification of halite crystallization events on seasonal basis using Athens-Hellinikon HNMS station data, in the period 1980–2004. Black squares indicate winter (DJF) values, green circles spring (MAM), grey triangles summer (JJA) and red diamonds autumn (SON).

3.3. Mineralogical and Microstructural Characterization

The mineralogical, petrographic and microstructural examination revealed that all seven samples belong to the same type of rock formation, the so-called Marl of Piraeus. The

mineralogical analysis (XRD) of the reference samples highlighted the presence of calcite (**C**: $CaCO_3$) as the main mineralogical phase, along with the minor phases of dolomite (**D:** $CaMg(CO_3)_2$), quartz (**Q:** SiO_2), albite (**A:** $NaAlSi_3O$) and the clay minerals illite (**I:** $(K,H_3O)(Al,Mg,Fe)_2(Si,Al)_4O_{10}[(OH)_2,(H_2O)]$), and kaolinite/montmorillonite (K/M: $Al_2Si_2O_5(OH)_4/(Na,Ca)_{0.33}(Al,Mg)_2(Si_4O_{10})(OH)_2 \bullet nH_2O$) are also detected (Figure 5). The presence of clay minerals in the case of S_05 and S_06 can also be detected macroscopically due to the presence of yellowish veins that come across the bedding layers of the stones. This yellowish hue (Figure 6) is attributed to the presence of iron oxides [26].

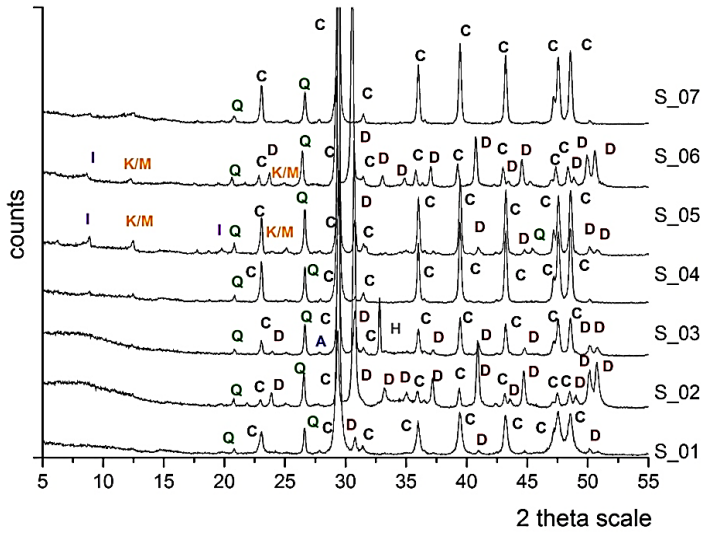


Figure 5. X-ray diffraction patterns of the seven untreated natural stone samples, indicating the presence of calcite (**C**), dolomite (**D**), quartz (**Q**), albite (**A**), illite (**I**), kaolinite/montmorillonite (**K/M**) and halite (**H**).

The seven stone samples are characterized as calcareous sediments, with an increased amount of clay content (15%) and a mesoporous structure with low connectivity. The micritic matrix of all seven samples is characterized by the presence of microfossils (ooids) and veins that come across the mass of the stone and are filled with secondary deposited sparritic calcite (Figure 6 SEM microphotographs). The stone samples can be categorized as fossiliferous biomicrite marls.

Specifically, S_01 was a whitish marly limestone with coherent micritic structure, rich in ooids, with intergranural and vuggy porosity. S_02 was a pale yellow marly limestone with coherent micritic structure, characterized by the presence of intergranural and vuggy porosity, along with moldic porosity (secondary porosity). It was characterized by the presence of salts on the superficial layers and by the presence of cracks. S_03 was a yellowish marly limestone with micritic structure, presenting intrafossil pores (intragranural porosity) and moldic porosity, in addition to intergranural and vuggy porosity. Calcite veins were also detected and attributed to the presence of the phenomena of differential erosion. S_04 was a pale yellow marly limestone with coherent micritic structure, presenting intrafossil pores (intragranural porosity), in addition to intergranural and vuggy porosity. The matrix of S_03 and S_04 was characterized by the enhanced presence of ooids and benthic foraminifera. S_05 and S_06 were whitish marly limestones with coherent micritic structure, characterized macroscopically by the presence of extended yellowish layers composed of clay minerals that were previously identified. Both stones presented vuggy and moldic porosity. The stone matrix presented large areas of colour alterations. S_07 was a pale yellow marly limestone with coherent micritic structure, presenting intrafossil pores (intragranural porosity), in addition to intergranural and vuggy porosity (Figure 6). The matrix was characterized by the enhanced presence of ooids and benthic foraminifera [53,54].

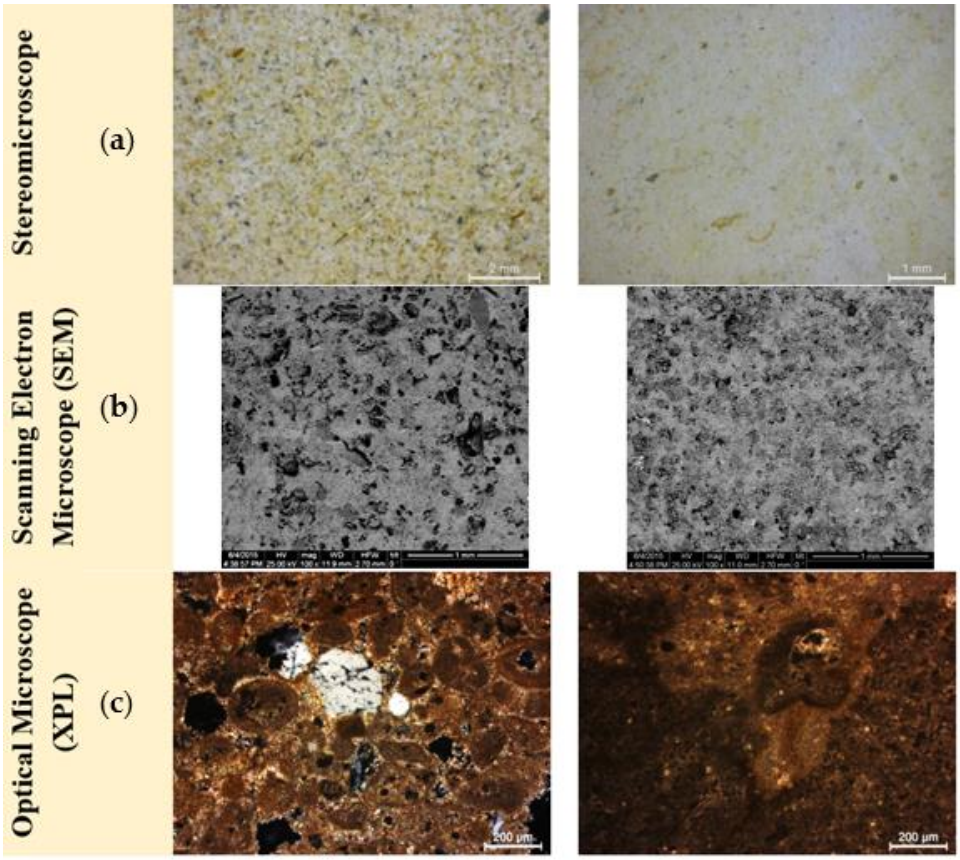


Figure 6. Microstructural and petrographic characteristics of representative samples from the seven untreated stone samples in (**a**) S_04 and S_05 in stereomicroscope (scale bar at 2 mm and 1 mm), (**b**) S_02 and S_07 in SEM microscope (BSE) (scale bar at 1 mm) and (**c**) S_04 and S_05 in optical microscope (XPL) (scale bar at 200 μm).

The estimated values of open porosity, the coefficient of capillary water absorption and mechanical properties vary significantly due to the differentiations attributed to the stratification of the natural stones (Table 1). S_05 and S_07 presented increased values of open porosity (37.9% and 29.7%, respectively), whereas S_02 and S_03 presented increased values of the coefficient of capillary water absorption (0.11 kg/m^2 s$^{0.5}$ and 0.12 kg/m^{2}s$^{0.5}$, respectively). As far as the mechanical properties are concerned, S_01 presented the highest values, whereas S_07 presented a significant lack of flexural strength. The total conductivity measurements of the untreated stone samples vary from 350–4500 μS/cm, indicating the presence of soluble salts, specifically halite (H: NaCl), which was also detected in the mineralogical analysis (Figure 5).

3.4. Evaluation of Conservation Treatments

The microstructural characteristics of both untreated and treated stone specimens were examined with the use of SEM (Figure 7). The two representative microphotographs of the untreated stone samples indicated sparritic and micritic calcite crystals (n.9 and n.10, respectively, in Figure 7a) and the presence of clay minerals (n.11 in Figure 7b). Upon the completion of the polymerization reaction after the time period of eight weeks, the comparative evaluation of the deposition and formation of the end-products of the polymerization reaction underlined that, in all cases, the deposited material was distributed rather unevenly on the grains and inside the pores of the material. The resulting product of the polymerization reaction of the two consolidants **OH-100** (Figure 7c) and **KS 300HV** (Figure 7e) was a dense thick silica gel that proved to cover the surface of grains and partially fill the pores, forming small "connections" between them (n.12 in Figure 7e). The

silica gel was characterized in both cases by the occurrence of cracks along the newly formed material, generated by the high capillary pressure from the gel network during drying (n.13 in Figure 7c,e) [55]. In the case of the two water repellents **Funcosil SL** (Figure 7d) and **BS 1001** (Figure 7f), material was deposited on and in-between the grains and the pores of the porous substrate forming a non-continuous hydrophobic film (n.12), characterized by the presence of cracks (n.13).

Table 1. Physical and mechanical properties of all seven natural stone samples of the marly limestone of the Hellenistic theater of Zea.

Samples	Open Porosity %	Mean Pore Radius (μm)		Mode Pore Radius (μm)	
		High Pressure	Low Pressure	High Pressure	Low Pressure
S_01	19.5	0.03	0.03	0.002	-
S_02	22.2	0.04	50.35	0.02	5.35
S_03	22.7	0.09	23.35	0.024	5.36
S_04	25.6	0.05	14.63	0.003	5.35
S_05	37.9	0.08	57.75	0.011	7.078
S_06	22.2	0.08	47.11	0.015	6.313
S_07	29.7	0.03	13.58	0.002	5.340

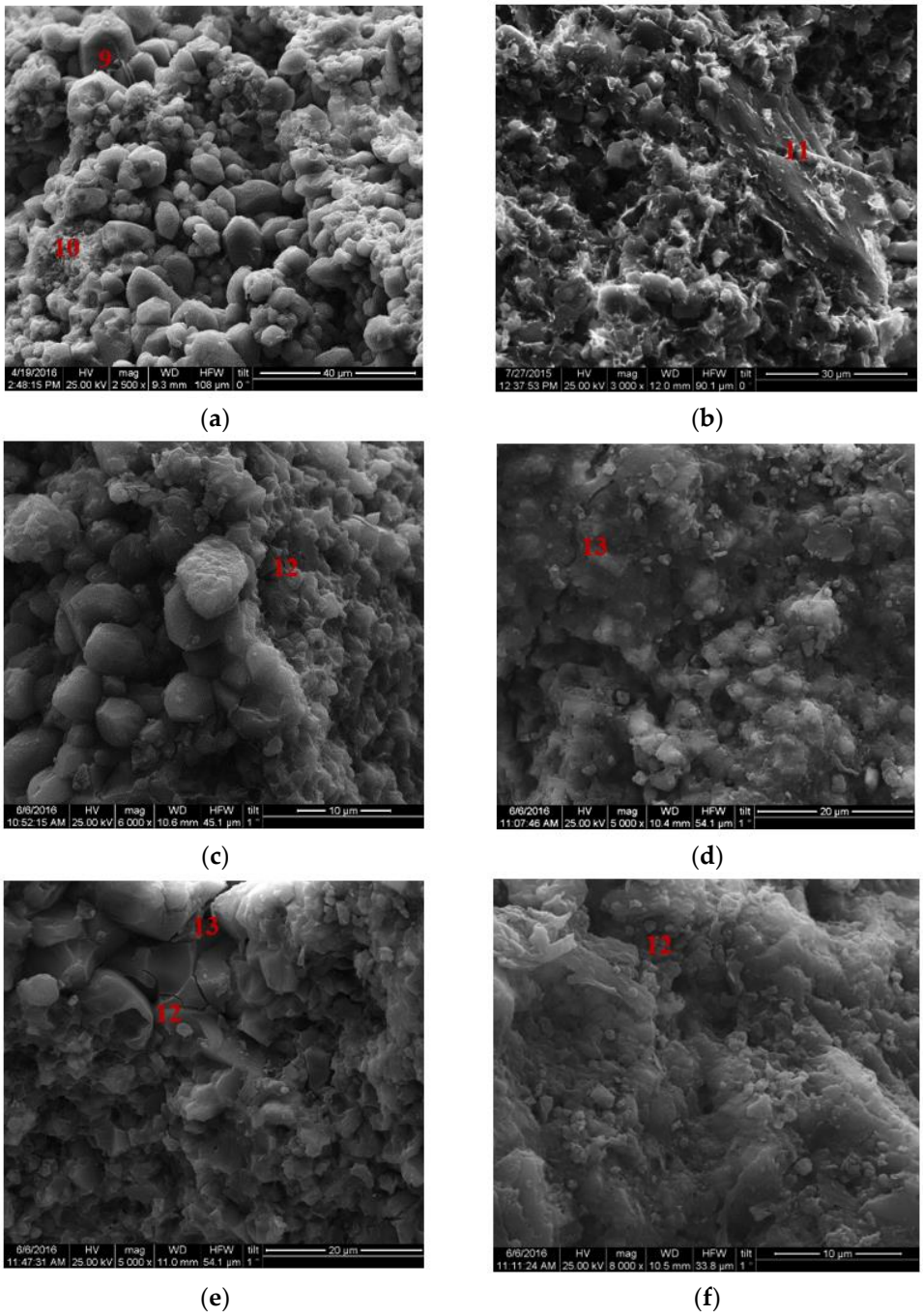
Samples	Capillary Water Absorption Coefficient (A_{cap}) ($kg/m^2\ s^{0.5}$)	Conductivity (mS/cm)	3 Point Bending Strength (Mpa)	Compressive Strength (MPa)
S_01	0.02	3.5	12	62.1
S_02	0.09	4.4	1.8	32.8
S_03	0.11	1.5	5.5	29
S_04	0.13	0.8	4	18.9
S_05	0.07	0.4	-	5.7
S_06	0.07	0.8	3.8	14.6
S_07	0.04	-	5.4	46.5

The comparison of the open porosity between untreated and treated stone specimens proved the evident reduction of the open porosity due to the material deposited after the treatments in the cases of S_01, S_05, S_06 and S_07 (Figure 8a), whereas in the cases of S_02, S_03 and S_04, a slight reduction of the open porosity was detected (Figure 8a). Specifically, in S_01, the open porosity was varied in the range of 7.3% to 14.9%, compared to the initial values of 19.5%. In S_05, the open porosity was reduced from 37.9% to a range from 12.7% to 23.0%; in S_06, the open porosity was reduced from 22.2% to a range from 11.5% to 17.3%; and in S_07, the open porosity was reduced from 29.7% to a range from 4.5% to 12.9% (Figure 8a). In the case of the coefficient of water absorption by capillary Acap, the application of the two water repellents had a significant effect on the evident reduction of the Acap in all seven stones, causing the restraint of the estimated values of the treated stone sample at the range from 0.001 to 0.01 $kg/m^2s^{0.5}$ in all seven natural stones (Figure 8b).

3.5. Durability against Salt Weathering

The comparison of durability performance between untreated stone samples against salts weathering (Figure 9a) highlighted the low resistance of the stone samples S_05 and S_06, which was evident from the continuous weight loss and the consequent fast

degradation rate that led to their collapse during the 5th and 6th cycle, respectively. In contrast, the performance of S_01, S_02 and S_07 was characterized by a slow degradation rate because they presented an initial weight gain due to the accumulation of NaCl, which was gradually altered to slight weight loss and collapse at the final cycle.

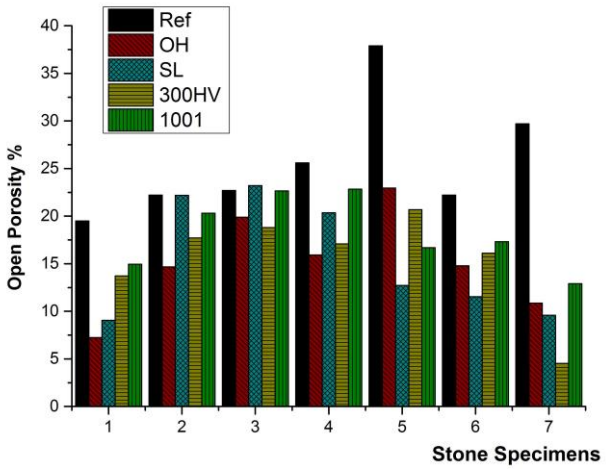


(**a**) (**b**) (**c**) (**d**) (**e**) (**f**)

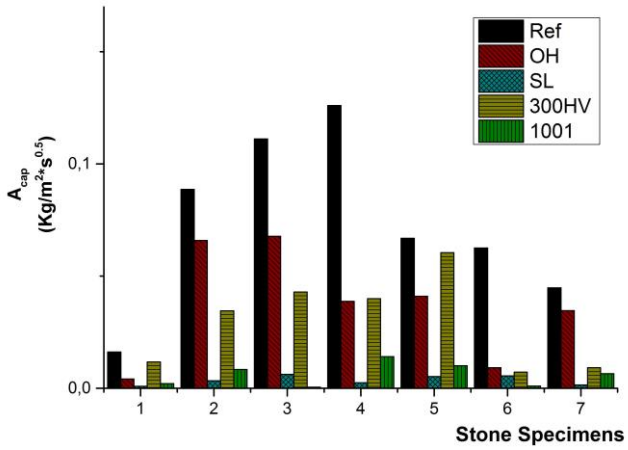
Figure 7. SEM microphotographs of representative stone samples: (**a**) untreated bulk stone (scale bar at 40 μm); (**b**) presence of alumino-silicatic minerals (scale bar at 30 μm); (**c**) treated stone sample with **BS OH-100** (scale bar at 10 μm); (**d**) treated stone sample with **Funcosil SL** (scale bar at 20 μm); (**e**) treated stone sample with **KS 300HV** (scale bar at 20 μm) and (**f**) treated stone sample with **BS 1001** (scale bar at 20 μm).

The comparison of durability performance between untreated and treated stone samples highlighted that all four treatments resulted in the reduction of the degradation rate due to salt weathering. All treated stones presented an initial weight gain due to accumu-

lation of NaCl. Specifically, in the case of S_01 (Figure 9b), the untreated specimen was the only one that presented a small weight loss after the 24th cycle, whereas the treated stone specimen with **KSE 300HV** presented a continuous weight gain. In the cases of both S_02 (Figure 9c) and S_03 (Figure 9d), both the untreated stone sample and that treated with **BS OH 100** presented gradual weight loss after the 10th and 20th cycle, respectively, which led to material loss. In the case of S_04 (Figure 9e), the untreated specimen was the only one that presented a gradual weight loss after the 10th cycle. In the case of S_05 (Figure 9f), the untreated stone sample, along with the stone samples that were treated with the two consolidants **BS OH 100** and **KSE 300HV,** presented an enhanced degradation rate through the abrupt weight reduction and material collapse after the 5th cycle, whereas only the treated stone specimen with **FUNCOSIL SL** presented an increased resistance towards salt weathering when compared to the other four specimens from S_05. In the case of S_06 (Figure 9g), the untreated stone sample collapsed at the 5th cycle, and that treated with **BS OH 100** and **BS 100** presented a gradually weight loss after the 8th and 22th cycle, respectively, which led to material loss and collapse. In the case of S_07 (Figure 9h), the untreated specimen was the only one that presented a small weight loss after the 28th cycle.



(**a**)



(**b**)

Figure 8. Schematic representation of the effect of the conservation treatments on: (**a**) the open porosity and (**b**) capillary water absorption coefficient (Acap).

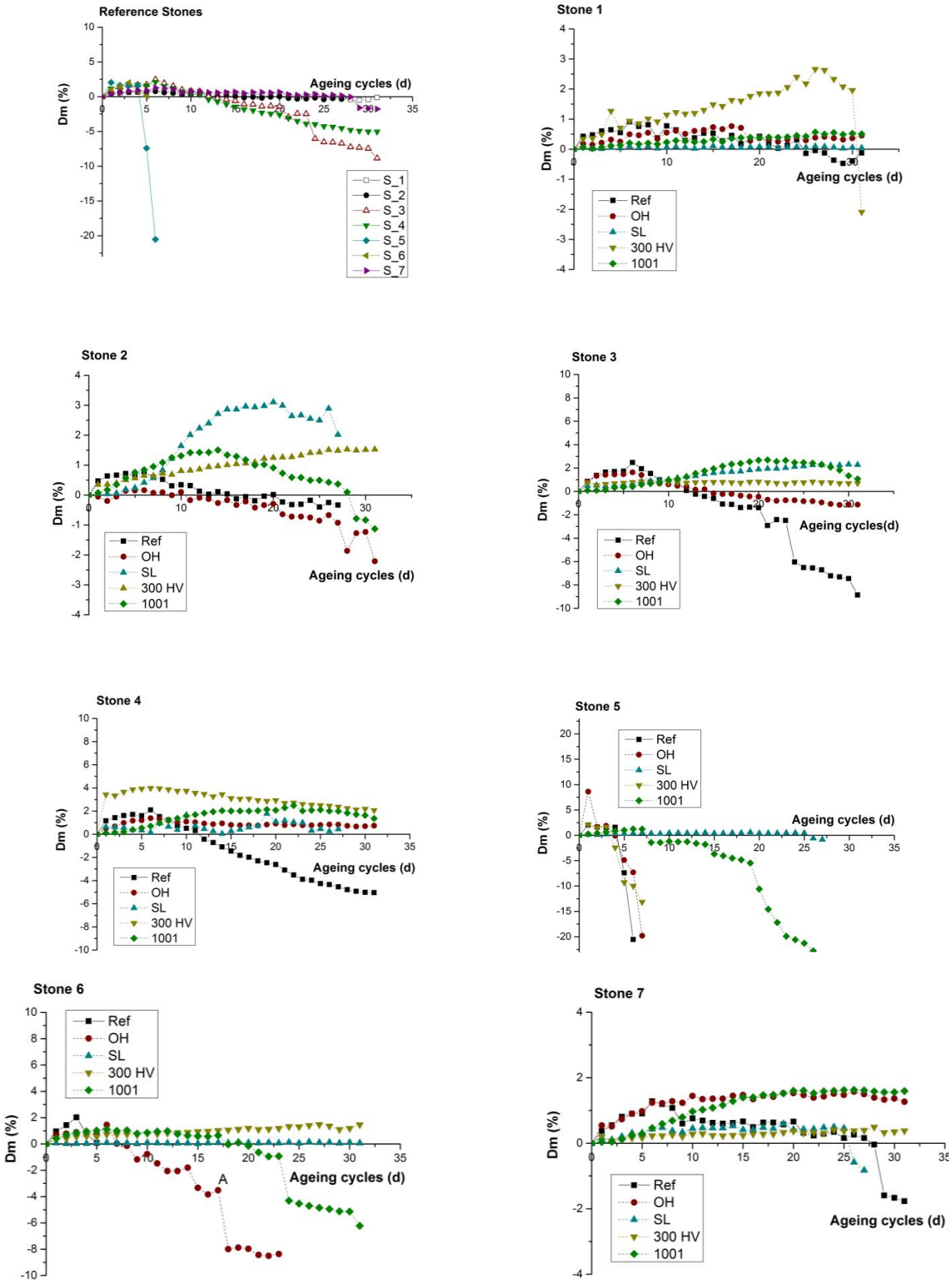
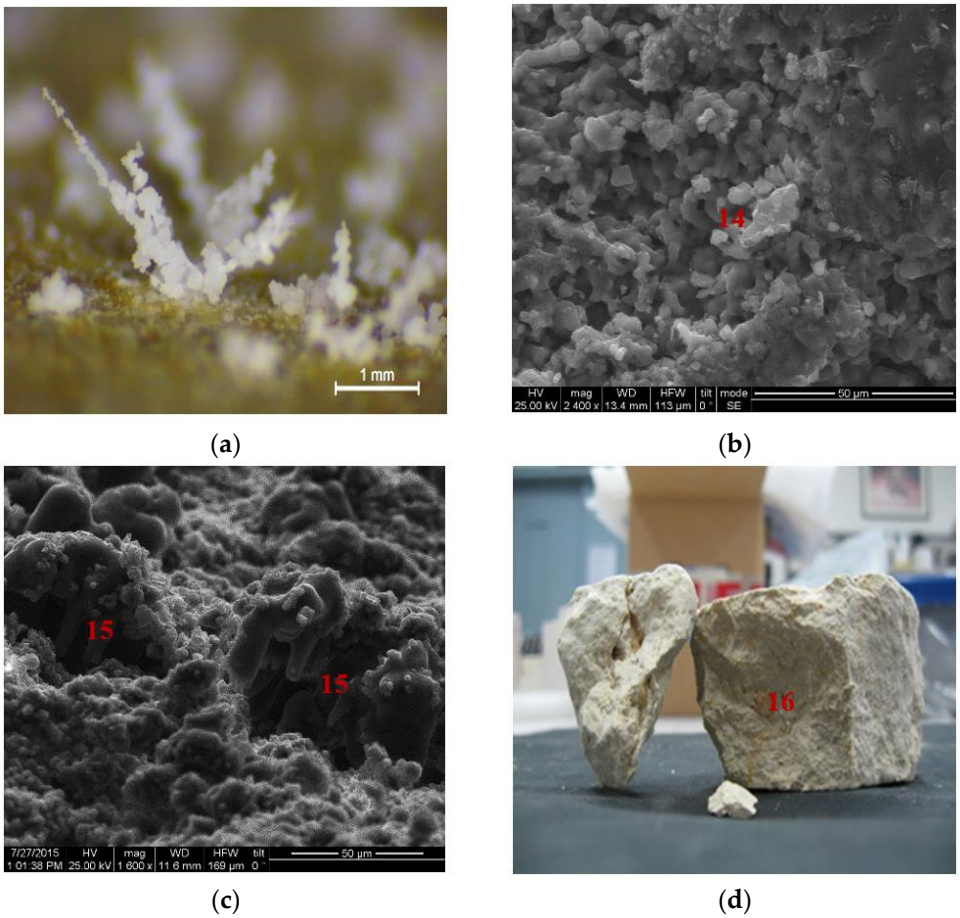


Figure 9. Weight difference (ΔW%) of both treated and untreated stone samples during the 31 operation cycles (days).

Salt weathering exhibited different patterns, such as efflorescence (Figure 10a,b), (n.14 in Figure 10b) and flaking (n.15 in Figure 10c), along with clay swelling phenomena (n.16 in Figure 10d).



(**a**) (**b**) (**c**) (**d**)

Figure 10. Microstructural and petrographic characteristics of the seven untreated stone samples in (**a**) salts attributed to occurrence of efflorescence on the stone surface (Stereomicroscope, scale bar at 1 mm); (**b**) deposition of NaCl crystallization causing eventually the appearance of cracking phenomena (SEM microphotographs, scale bar at 50 µm); (**c**) mechanical damage due to NaCl crystallization causing efflorescence (SEM microphotographs, scale bar at 50 µm) and (**d**) cracking of the stone specimen attributed to the synergetic effect of rich alumino-silicatic composition and accelerating ageing tests.

4. Discussion

The elaboration of the results from the in situ survey (Figure 3) and the seasonal quantification of halite crystallization events (Figure 4) highlighted soluble salts crystallization as the primary deterioration agent. The thermodynamics of halite's energy equilibrium (and the consequent effect on the phenomena of dissolution/crystallization/hydration) are generally affected by environmental conditions [56,57]. The main environmental factor that has proven to have a direct effect on the realization of the crystallization process was the high values of RH during winter and spring. As crystallization is an evaporation driven process [57], the relative slow evaporation rate due to the microclimate of the monument could be connected to the presence of sub-fluorescence and scaling phenomena resulting from the crystallization of halite inside the porous substrate. Simultaneously, the decreased temperature values reported during the winter contribute to the increase of the supersaturation of the solution and, thus, the crystallization of halite. Overall, the combined action of RH and temperature fluctuations in the outdoor environment create a hygrothermal environment that promotes the presence of additional stresses to the stone materials [58–62].

The correlation between the local microclimate (specifically its seasonal and annual variations) and the weathering phenomena is the basis for the vulnerability assessment and for predicting and developing an adaptation plan against the effects of climate change, while highlighting the need for prioritizing salt crystallization as one of the most common risk factors for cultural heritage monuments in coastal archaeological contexts.

The elaboration of the results obtained through the petrographic, microstructural and mineralogical examination of the seven untreated natural stone samples was in accordance with the weathering phenomena that were identified during in situ inspection of the archaeological site. Specifically, the weathering phenomena were attributed to the synergistic effect of water-related phenomena, such as the enhanced action of salt crystallization and marine aerosol phenomena, along with the characteristics of the pore space of the marly limestone and the presence of clay minerals.

The enhanced presence of capillary pores was connected with the increased values of the coefficient of water absorption by capillarity Acap, indicating the rapid water uptake of sufficient amounts of water inside the pore space and the consequent mobilization of salts [63]. Moreover, the estimated size of meso-pores suggested that the natural stones are susceptible to salt weathering because the pressure applied on the walls of the stones cannot be reduced, as in the case of macro-pores [64]. The intense reduction of the coefficient of water absorption by capillarity Acap in the case of the two water repellents FUNCOSIL SL and BS 1001 contributed to the durability enhancement of the stone samples (Figure 7). In the case of the two silicatic consolidants, BS OH 1000 and KSE 300HV, the enhanced adhesion between the resulting product of the polymerization reaction and the silicatic components of the stone led to the increase of the internal cohesion of the natural stones through the reduction of the open porosity (Figures 7 and 8). The modification of the microstructure of the treated stone specimens indicated that the future in situ application of conservation treatments (both consolidation products and water repellents) should be done homogeneously to avoid the presence of weathering phenomena induced on the untreated part of the stone.

Furthermore, the presence of clay minerals of the smectite group (Figures 5 and 10) on stone specimens S_05 and S_06 facilitated the swelling phenomenon due to the absorption of water molecules and/or soluble salts that led to the expansion of the inter-layer, thus initiating internal stresses and crack formation [65–67] and, therefore, the material collapse at the early cycles of the salt weathering test.

Overall, all four conservation treatments result in the increase of stone resistance to salt weathering (Figure 9), either by increasing the internal cohesion [68] with the partial filling of the pores with silica gel through the application of the two consolidants BS OH 1000 and KSE 300HV (Figure 7a), or through hydrophobization of the layers close to the stone surface with the use of the two water-repellents FUNCOSIL SL and BS 1001 (Figure 7a,b). The comparative evaluation of the durability of the treated samples (Figure 9) presented a slight increase of weight loss in the case of BS OH 1000, which could be attributed to the production of increased values of crystallization pressure [69]. Furthermore, in the case of S_05 with increased clay content, the hydrophobization effect attributed to the water-repellents FUNCOSIL SL and BS 1001, proved to present anti-swelling capacity, through the reduction of the accessibility of water content inside the stone mass, without the presence of the consequent phenomenon of the accumulation of salts on the surface of the stone.

5. Conclusions

The elaboration of the results revealed that the design of migration actions proved to be multivariable parameters: the microstructural and mineralogical characterization of the stone samples, the environmental parameters of local microclimate and the efficacy (internal cohesion and partial hydrophobization). Specifically:

- Both in situ and laboratory examination of the archaeological weathered stone samples of the Hellenistic theater of Zea highlighted water and soluble salts (NaCl) as the key parameters for the vulnerability of marly limestone.

- Past and current climate data indicated the continuous presence of an elevated number of annual crystallization events that maintain a very high risk for the natural stones of the Zea theater.
- The microstructural characteristics of the natural stone, such as the mesoporous structure characterized by low porous connectivity, contribute to the enhancement of the weathering phenomena, induced mainly by either the deposition of salts on the superficial layers or the absorption and circulation of water of high salt content inside the stone mass, enhanced by the microclimate conditions of the outdoor monument. The presence of swelling clays proved to increase the susceptibility of the marly limestone to water.
- In terms of adhesion, the two silane-based consolidants **BS OH 100** and **KSE 300HV** present sufficient adhesion with the silicatic stone components, whereas the two water repellents **FUNCOSIL SL** and **BS 1001** proved to form a non-continuous hydrophobic film in-between grains and inside the pores. The consolidant **KSE 300HV** and the two water repellents **FUNCOSIL SL** and **BS 1001** proved to enhance the durability of the stone against salt weathering and to reduce the open porosity of the stone samples, improving the internal cohesion of the stone mass.
- Consolidation and hydrophobicity treatments proved to have a beneficial effect on the durability against salts crystallization, while the consolidant **KSE 300HV** and the two water repellents **FUNCOSIL SL** and **BS 1001** exhibited the most promising results. The results suggested that a future in situ application of the conservation treatments should be implemented homogenously in order to avoid the presence of weathering phenomena induced on the untreated part of the stones.

Author Contributions: Conceptualization, A.M., V.K. and I.K.; methodology, A.M., D.V. and I.K.; investigation, A.M. and I.M.; data curation, A.M. and I.M.; writing—original draft preparation, A.M., D.V., V.K. and I.K.; writing—review and editing, A.M., I.M., D.V., A.S., V.K. and I.K. All authors have read and agreed to the published version of the manuscript.

Funding: This research received no external funding.

Institutional Review Board Statement: Not applicable.

Informed Consent Statement: Not applicable.

Data Availability Statement: Not applicable.

Acknowledgments: We acknowledge the support of this work by the project "Development of Materials and Devices for Industrial, Health, Environmental and Cultural Applications" (MIS 5002567), which is implemented under the "Action for the Strategic Development on the Research and Technological Sector", funded by the Operation-al Programme "Competitiveness, Entrepreneurship and Innovation" (NSRF 2014–2020) and co-financed by Greece and the European Union (European Regional Development Fund). The authors would like to acknowledge the director of Ephorate of Antiquities of Piraeus and the Islands Department, S. Chryssoulaki, and the lead archaeologist, M. Giamalidis.

Conflicts of Interest: The authors declare no conflict of interest.

References

1. Bonomo, A.E.; Amodio, A.M.; Prossera, G.; Sileo, M.; Rizzo, G. Evaluation of soft limestone degradation in the Sassi UNESCO site (Matera, Southern Italy): Loss of material measurement and classification. *J. Cult. Herit.* **2020**, *42*, 191–201. [CrossRef]
2. Grossi, C.M.; Brimblecombe, P.; Menéndez, B.; Benavente, D.; Harris, I.; Déqué, M. Climatology of salt transitions and implications for stone weathering. *Sci. Total Environ.* **2011**, *409*, 2577–2585. [CrossRef]
3. Bonazza, A.; Messina, P.; Sabbioni, C.; Grossi, C.M.; Brimblecombe, P. Mapping the impact of climate change on surface recession of carbonate buildings in Europe. *Sci. Total Environ.* **2009**, *407*, 2039–2050. [CrossRef] [PubMed]
4. Manohar, S.; Bala, K.; Santhanam, M.; Menon, A. Characteristics and deterioration mechanisms in coral stones used in a historical monument in a saline environment. *Constr. Build. Mater.* **2020**, *241*, 118102. [CrossRef]

5. Anzani, A.; Cardani, G.; Condoleo, P.; Garavaglia, E.; Saisi, A.; Tedeschi, C.; Tibaroschi, C.; Valluzzi, M.R. Understanding of historical masonry for conservation approaches: The contribution of Prof. Luigia Binda to research advancement. *Mater. Struct. Constr.* **2018**, *51*, 1–27. [CrossRef]
6. Apostolopoulou, M.; Keramidas, V.; Galanaki, N.; Kalofonou, M.; Skoula, C.; Karoglou, M.; Delegou, E.T.; Mouzakis, C.; Bakolas, A.; Moropoulou, A.; et al. A Study on the Historical Materials of the Apollo Pythios Temple in Rhodes and the Evaluation of Potential Restoration Materials. *Heritage* **2019**, *2*, 988–1022. [CrossRef]
7. Ortiz, P.; Artunez, V.; Martin, J.M.; Ortiz, R.; Vasquez, M.A.; Galan, E. Approach to environmental risk analysis for the main monuments in a historical city. *J. Cult. Herit.* **2014**, *15*, 432–440. [CrossRef]
8. Szczepaniak, M. Rock materials in monuments and archaeology–research methods. In *Geoscience in Archaeometry. Methods and Case Studies*; Michalska, D., Szczepaniak, M., Eds.; Bogucki Wydawnictwo Naukowe Publisher: Poznan, Poland, 2014; pp. 13–36.
9. Patil, S.M.; Kasthurba, A.K.; Patil Mahesh, V. Characterization and assessment of stone deterioration on Heritage Buildings. *Case Stud. Constr. Mater.* **2021**, *15*, e00696. [CrossRef]
10. Snethlage, R. Natural Stones in Architecture: Introduction. In *Stone in Architecture Properties, Durability XII*; Siegesmund, S., Snethlage, R., Eds.; Springer: Berlin/Heidelberg, Germany, 2011; Volume 552, pp. 1–9.
11. Raju, K.; Ravindhar, S. Detailed review on natural stone materials in architecture. *Mater. Today Proc.* **2021**, *45*, 6341–6347. [CrossRef]
12. Martínez-Martínez, J.; Arizzi, A.; Benavente, D. The Role of Calcite Dissolution and Halite Thermal Expansion as Secondary Salt Weathering Mechanisms of Calcite-Bearing Rocks in Marine Environments. *Minerals* **2021**, *11*, 911. [CrossRef]
13. Caroll, P.; Aarrevaara, E. Review of Potential Risk Factors of Cultural Heritage Sites and Initial Modelling for Adaptation to Climate Change. *Geosciences* **2018**, *8*, 322. [CrossRef]
14. Re, G.; Croce, A.; D'Angelo, D.; Marchese, L.; Rinaudo, C.; Gatti, G. Application of nano-coating technology for the protection of natural lapideous materials. *Surf. Coat. Technol.* **2022**, *441*, 128507. [CrossRef]
15. Hatir, M.E.; Barstugari, M.; Incec, I. Deep learning-based weathering type recognition in historical stone monuments. *J. Cult. Herit.* **2020**, *45*, 193–203. [CrossRef]
16. Sesana, E.; Gagnon, A.S.; Ciantelli, C.; Cassar, J.A.; Hughes, J.J. Climate change impacts on cultural heritage: A literature review. *Clim. Change* **2021**, *12*, e710. [CrossRef]
17. Spezziano, P. Mapping the susceptibility of UNESCO World Cultural Heritage sites in Europe to ambient (outdoor) air pollution. *Sci. Total Environ.* **2021**, *754*, 142345. [CrossRef]
18. Sardella, A.; Palazzi, E.; von Hardenberg, J.; Del Grande, C.; De Nuntiis, P.; Sabbioni, C.; Bonazza, A. Risk Mapping for the Sustainable Protection of Cultural Heritage in Extreme Changing Environments. *Atmosphere* **2020**, *11*, 700. [CrossRef]
19. Theodoridou, M.; Török, A. In situ investigation of stone heritage sites for conservation purposes: A case study of the Székesfehérvár Ruin Garden in Hungary. *Prog. Earth Planet. Sci.* **2019**, *6*, 15. [CrossRef]
20. Rodríguez-Rosales, B.; Abreu, D.; Ortiz, R.; Becerra, J.; Cepero-Acán, A.E.; Vázquez, M.A.; Ortiz, P. Risk and vulnerability assessment in coastal environments applied to heritage buildings in Havana (Cuba) and Cadiz (Spain). *Sci. Total Environ.* **2021**, *750*, 141617. [CrossRef]
21. Gibeaux, S.; Vázquez, P.; De Kock, T.; Cnudde, V.; Thomachot-Schneider, C. Weathering assessment under X-ray tomography of building stones exposed to acid atmospheres at current pollution rate. *Constr. Build. Mater.* **2018**, *168*, 187–198. [CrossRef]
22. Vecco, M.; Srakar, A. The unbearable sustainability of cultural heritage: An attempt to create an index of cultural heritage sustainability in conflict and war regions. *J. Cult. Herit.* **2018**, *33*, 293–302. [CrossRef]
23. Patil, S.M.; Kasthurba, A.K. Weathering of stone monuments: Damage assessment of basalt and laterite. *Mater. Today Proc.* **2021**, *43*, 1647–1658. [CrossRef]
24. Molina, E.; Cultrone, G.; Sebastián, E.; Alonso, F.J.; Carrizo, L.; Gisbert, J.; Buj, O. The pore system of sedimentary rocks as a key factor in the durability of building materials. *Eng. Geol.* **2011**, *118*, 110–121. [CrossRef]
25. Cardell, C.; Delalieux, F.; Roumpopoulos, K.; Moropoulou, A.; Auger, F.; Van Grieken, R. Salt-induced decay in calcareous stone monuments and buildings in a marine environment in SW France. *Constr. Build. Mater.* **2003**, *17*, 165–179. [CrossRef]
26. Michalopoulou, A.; Sioulas, D.; Amenta, M.; Kilikoglou, V.; Karatasios, I. Variable Weathering Response of Architectural Marlstones Against NaCl Crystallization. In *10th International Symposium on the Conservation of Monuments in the Mediterranean Basin. MONUBASIN 2017*; Koui, M., Zezza, F., Kouis, D., Eds.; Springer: Berlin/Heidelberg, Germany, 2018; pp. 347–355. [CrossRef]
27. Theoulakis, P.; Moropoulou, A. Microstructural and mechanical parameters determining the susceptibility of porous building stones to salt decay. *Constr. Build. Mater.* **1997**, *11*, 65–71. [CrossRef]
28. Stefanis, N.A.; Theoulakis, P.; Pilinis, C. Dry deposition effect of marine aerosol to the building stone of the medieval city of Rhodes, Greece. *Build. Environ.* **2009**, *44*, 260–270. [CrossRef]
29. Zezza, F.; Macri, F. Marinea erosol and stone decay. *Sci. Total Environ.* **1995**, *167*, 123–143. [CrossRef]
30. Zornoza-Indart, A.; Lopez-Arce, P.; Zoghlami, K.; Leal, N.; Simão, J. Marine Aerosol Weathering of Mediterranean Calcarenite Stone: Durability of Ethyl Silicate, Nano $Ca(OH)_2$, Nano SiO_2, and Nanostructured Consolidating Products. *Studi. Con.* **2019**, *64*, 73–89. [CrossRef]
31. Rodriguez-Navarro, C.; Doehne, E.; Sebastian, E. Origins of honeycomb weathering: The role of salts and wind. *GSA Bull.* **1999**, *111*, 1250–1255. [CrossRef]

32. Lopez-Arce, P.; Garcia-Guinea, J.; Benavente, D.; Tormo, L.; Doehne, E. Deterioration of dolostone by magnesium sulphate salt: An example of incompatible building materials at Bonaval Monastery, Spain. *Constr. Build. Mater.* **2009**, *23*, 846–855. [CrossRef]
33. Morillas, H.; Maguregui, M.; Gallego-Cartagena, E.; Marcaida, I.; Carral, N.; Madariaga, J.M. The influence of marine environment on the conservation state of Built Heritage: An overview study. *Sci. Total Environ.* **2020**, *745*, 140899. [CrossRef]
34. Sirbu, R.; Negreanu-Pirjol, T.; Sirbu, M.; Cadar, E.M. Aggressivity of the marine medium in some buildings from the Romanian Black Sea coast. *J. Environ. Prot. Ecol.* **2006**, *7*, 59–68.
35. Azeroual, M.; Baghdad, B.; Bounakhla, M.; Doukkali, A.; El Wartiti, M. The atmospheric pollution and the marine aerosols impact on the monumental stone of the Sale surrounding wall's entrances (Morroco). *Phys. Chem. News* **2007**, *33*, 59–64.
36. Costa, E.A.L.; Campos, V.P.; da Silva Filho, L.C.P.; Greven, H.A. Evaluation of the aggressive potential of marine chloride and sulfate salts on mortars applied as renders in the Metropolitan Region of Salvador-Bahia, Brazil. *J. Environ. Manag.* **2008**, *90*, 1060–1068. [CrossRef]
37. Flatt, R.J. Salt damage in porous materials: How high supersaturations are generated. *J. Cryst. Growth* **2002**, *242*, 435–455. [CrossRef]
38. Lubelli, B.; van Hees, R.P.J. *Evaluation of the Effect of Nano-Coatings with Water Repellent Properties on the Absorption and Drying Behaviour of Brick IN Hydrophobe VI 6th International Conference on Water Repellent Treatment of Building Materials*; Fassina, V., Ed.; Aedificatio Publishers: Rome, Italy, 2011; pp. 125–136.
39. Steiger, M. Crystal growth in porous materials: I. The crystallization pressure of large crystals. *J. Cryst. Growth* **2005**, *282*, 455–469. [CrossRef]
40. Zornoza-Indart, A.; Lopez-Arce, P. 3—Stone. In *Long-Term Performance and Durability of Masonry Structures*; Ghiassi, B., Lourenço, P.B., Eds.; Woodhead Publishing Series in Civil and Structural Engineering; Woodhead Publishing: Cambridge, UK, 2019; pp. 59–88. [CrossRef]
41. Apostolopoulos, G.; Pavlopoulos, K.; Goiran, J.-P.; Fouache, E. Was the Piraeus peninsula (Greece) a rocky island? Detection of pre-Holocene rocky relief with borehole data and resistivity tomography analysis. *J. Archaeol. Sci.* **2014**, *42*, 412–421. [CrossRef]
42. Goiran, J.-P.; Pavlopoulos, K.; Fouache, E.; Triantaphyllou, M.; Etienne, R. Piraeus, the ancient island of Athens: Evidence from Holocene sediments and historical archives. *Geology* **2011**, *39*, 531–534. [CrossRef]
43. Cai, Y.; Hou, P.; Duan, C.; Zhang, R.; Zhou, Z.; Cheng, Z.; Shah, S. (The use of tetraethyl orthosilicate silane (TEOS) for surface-treatment of hardened cement-based materials: A comparison study with normal treatment agents. *Constr. Build. Mater.* **2016**, *117*, 144–151. [CrossRef]
44. Adamopoulos, F.G.; Vouvoudi, E.C.; Pavlidou, E.; Achilias, D.S.; Karapanagiotis, I. TEOS-Based Superhydrophobic Coating for the Protection of Stone-Built Cultural Heritage. *Coatings* **2021**, *11*, 135. [CrossRef]
45. Sena da Fonseca, B.; Ferreira Pinto, A.P.; Piçarra, S.; Montemor, M.F. Alkoxysilane-based sols for consolidation of carbonate stones: Proposal of methodology to support the design and development of new consolidants. *J. Cult. Herit.* **2020**, *43*, 51–63. [CrossRef]
46. Briffa, S.M.; Vella, D.A. The behaviour of as-applied and artificially weathered silica–epoxy consolidants on a typical Mediterranean porous limestone: A comparison with TEOS. *Herit. Sci.* **2019**, *7*, 1–13. [CrossRef]
47. Gemelli, G.M.C.; Zarzuela, R.; Alarcón-Castellano, F.; Mosquera, M.J.; Almoraima Gil, M.L. Alkoxysilane-based consolidation treatments: Laboratory and 3-years In-Situ assessment tests on biocalcarenite stone from Roman Theatre (Cádiz). *Constr. Build. Mater.* **2021**, *312*, 125398. [CrossRef]
48. Ban, M.; De Kock, T.; Ott, F.; Barone, G.; Rohatsch, A.; Raneri, S. Neutron Radiography Study of Laboratory Ageing and Treatment Applications with Stone Consolidants. *Nanomaterials* **2019**, *9*, 635. [CrossRef] [PubMed]
49. Ferreira Pinto, A.P.; Delgado Rodrigues, J. Impacts of consolidation procedures on colour and absorption kinetics of carbonate stones. *Stud. Conserv.* **2014**, *59*, 79–90. [CrossRef]
50. Karatasios, I.; Michalopoulou, A.; Amenta, M.; Kilikoglou, V. Modification of water transport properties of porous building stones caused by polymerization of silicon-based consolidation products. *Pure. Appl. Chem.* **2017**, *89*, 1673–1684. [CrossRef]
51. Nunes, C.; Aguilar Sanchez, A.N.; Godts, S.; Gulotta, D.; Ioannou, I.; Lubelli, B.; Menendez, B.; Shahidzadeh, N.; Slížková, Z.; Theodoridou, M. Experimental research on salt contamination procedures and methods for assessment of the salt distribution. *Constr. Build. Mater.* **2021**, *298*, 123862. [CrossRef]
52. ICOMOS. *Illustrated Glossary of Stone Deterioration Patterns*; ICOMOS Open Archive: Petra, Jordan, 2001.
53. Choquette, P.W.; Pray, L.C. Geologic Nomenclature and Classification of Porosity in Sedimentary Carbonates. *AAPG Bull.* **1970**, *54*, 207–250.
54. Fournier, F.; Pellerin, M.; Villeneuve, Q.; Teillet, T.; Hong, F.; Poli, E.; Borgomano, J.; Léonide, P.; Hairabian, A. The Equivalent Pore Aspect Ratio as A Tool For Pore Type Prediction In Carbonate Reservoirs. *AAPG Bull.* **2018**, *102*, 1343–1377. [CrossRef]
55. Verganelaki, A.; Kilikoglou, V.; Karatasios, I.; Maravelaki-Kalaitzaki, P. A biomimetic approach to strengthen and protect construction materials witha novel calcium-oxalate–silica nanocomposite. *Constr. Build. Mat.* **2014**, *62*, 8–17. [CrossRef]
56. Bracciale, M.P.; Sammut, S.; Cassar, J.; Santarelli, M.L.; Marrocchi, A. Molecular Crystallization Inhibitors for Salt Damage Control in Porous Materials: An Overview. *Molecules* **2020**, *25*, 1873. [CrossRef]
57. Granneman, S.J.C.; Lubelli, B.; van Hees, R.B.J. Mitigating salt damage in building materials by the use of crystallization modifiers—A review and outlook. *J. Cult. Herit* **2019**, *40*, 183–194. [CrossRef]
58. Ferdyn-Grygierek, J.; Kaczmarczyk, J.M.; Blaszczok, J.M.; Lubina, P.; Koper, P.; Bulinska, A. Hygrothermal Risk in Museum Buildings Located in Moderate Climate. *Energies* **2020**, *13*, 344. [CrossRef]

59. Bot, I.K.; Bousahla, A.A.; Zemri, A.; Sekkal, M.; Kaci, M.; Bourada, A.; Tounsi, F.; Ghazwani, M.H.; Mahmoud, S.R. Effects of Pasternak foundation on the bending behavior of FG porous plates in hygrothermal environment. *Steel Compos. Struct.* **2022**, *43*, 821–837.
60. Cuong-Le, T.; Nguyen, K.D.; Hoang-Le, M.; Sang-To, T.; Phan-Vu, P.; Wahab, M.A. Nonlocal strain gradient IGA numerical solution for static bending, free vibration and buckling of sigmoid FG sandwich nanoplate. *Phys. B Condens. Mat.* **2022**, *631*, 413726. [CrossRef]
61. Yao, S.; Yan, Z.; Ma, Q.; Xu, B.; Zhang, Z.; Bi, W.; Zhang, J. Analysis of the annual hygrothermal environment in the Maijishan Grottoes by field measurements and numerical simulations. *Build. Environ.* **2022**, *221*, 109229. [CrossRef]
62. Martín-Garín, A.; Millán-García, J.A.; Terés-Zubiaga, J.; Oregi, X.; Rodríguez-Vidal, I.; Baïri, A. Improving Energy Performance of Historic Buildings through Hygrothermal Assessment of the Envelope. *Buildings* **2021**, *11*, 410. [CrossRef]
63. Snethlage, R. *Leitfaden Steinkonservierung*, 2nd ed.; Fraunhofer IRB Verlag: Stuttgart, Germany, 2005.
64. Benavente, D.; Sanchez-Moral, S.; Fernandez-Cortes, A.; Cavaneras, J.C.; Elez, J.; Saint-Jimenez, C. Salt damage and microclimate in the Postumius Tomb, Roman Necropolis of Carmona, Spain. *Environ. Earth Sci.* **2011**, *63*, 1529–1543. [CrossRef]
65. Benavente, D.; Such-Basañez, I.; Fernandez-Cortes, A.; Pla, C.; Cazorla-Amoros, D.; Cañaveras, J.C.; Sanchez-Moral, J.C. Comparative analysis of water condensate porosity using mercury intrusion porosimetry and nitrogen and water adsorption techniques in porous building stones. *Constr. Build. Mater.* **2021**, *288*, 123131. [CrossRef]
66. Tiennot, M.; Mertz, J.D.; Bourgès, A. Influence of clay minerals nature on the hydromechanical and fracture behaviour of Stones. *Rock Mech. Rock Eng.* **2019**, *52*, 1599–1611. [CrossRef]
67. Michalopoulou, A.; Maravelaki, N.; Stefanis, N.A.; Theoulakis, P.; Andreou, S.; Kilikoglou, V.; Karatasios, I. Evaluation of nanolime dispersions for the protection of archaeological clay-based building materials. *Mediterr. Archaeol. Archaeom.* **2020**, *20*, 221–242. [CrossRef]
68. Benavente, D.; García del Cura, M.A.; Bernabéu, A.; Ordóñez, S. Quantification of salt weathering in porous stones using an experimental continuous partial immersion method. *Eng. Geol.* **2001**, *59*, 313–325. [CrossRef]
69. Ruffolo, S.A.; Ricca, M.; Macchia, A.; La Russa, M.F. Antifouling coatings for underwater archaeological stone materials. *Prog. Org. Coat.* **2017**, *104*, 64–71. [CrossRef]

Disclaimer/Publisher's Note: The statements, opinions and data contained in all publications are solely those of the individual author(s) and contributor(s) and not of MDPI and/or the editor(s). MDPI and/or the editor(s) disclaim responsibility for any injury to people or property resulting from any ideas, methods, instructions or products referred to in the content.